

Holocene sediment budget and sedimentary history of the Ob and Yenisei estuaries

K. Dittmers*, F. Niessen, R. Stein

Alfred Wegener Institute for Polar and Marine Research, Columbusstrasse 2, 27568 Bremerhaven, Germany

Abstract

High-resolution acoustic data and several sediment gravity cores taken in the Ob and Yenisei estuaries allow us to balance the Holocene sediment budget of both rivers and to reconstruct their sedimentary history. Cores were radiocarbon dated and linked to acoustic profiles using whole-core physical properties.

The Ob and Yenisei estuaries, with their sea water fresh water mixing zone, act as major sediment sinks for fluvial derived terrigenous material in Holocene times. Most of the suspended and large amounts of dissolved matter precipitate in this zone termed "marginal filter". High thickness of Holocene sediments occurs between 72°N and 73°30'N where a distinct decrease in thickness is observed to the north. Two major acoustic units could be differentiated, separated by a prominent reflector interpreted as the base of the Holocene. High-resolution echosound data suggest a fluvial dominated depositional environment for the early Holocene displaying lateral accretion as point bars and vertical accreted overbank deposits in a fluvial channel-levee-complex. During the early Holocene sea-level rise the marginal filter migrated progressively southward (upstream) to its present position forming a typical high-stand system tract in acoustic images. Estuarine sedimentation in a sedimentary environment similar to today started at approximately 5 Cal. kyrs. BP. An estimated total of 14.3×10^{10} t and 9.2×10^{10} t of fine-grained brackish-marine sediments, in the Ob and Yenisei estuaries, respectively, were accumulated during Holocene times. This is only about 75% and about 50% of Ob and Yenisei estuarine sediment budgets, respectively, estimated by extrapolation of recent river run-off data over the last 7500 years. Filled paleoriver channels indicate active river incision in the southern part of the Kara Sea shelf prior to the Holocene.

1 Introduction

Sedimentation in the Arctic Ocean is dominated by terrigenous input which leads to high siliciclastic contents in marine sediments (Stein et al., 1994; Stein and Fahl, 2000). Biological productivity plays a minor role in sediment supply because the availability of nutrients is limited (Grebmeier, 1995). There are two major sources of terrigenous input: (i) riverine discharge which is prevailing in the western Arctic (MacDonald et al., 1998), and (ii) coastal erosion which is typical for the Laptev Sea (Rachold et al., 2000).

At present, total annual run-off sums up to 3330 km^3 for the whole Arctic. Approximately 30% of the Arctic Ocean fresh water input is supplied by the rivers Ob ($429 \text{ km}^3 \text{ y}^{-1}$) and Yenisei ($620 \text{ km}^3 \text{ y}^{-1}$) through their estuaries into the Kara Sea (Fig. 1; Aagaard and Carmack,

* corresponding author: kdittmers@awi-bremerhaven.de

1989; Gordeev et al., 1996). In total, rivers supply about $220 \cdot 10^6 \text{ t y}^{-1}$ of suspended matter to the Arctic Ocean (AMAP 1998). Despite their very large fresh water discharge rates (Shiklomanov and Skakalsky, 1994; Gordeev et al., 1996), the mean sediment yield of up to $22 \cdot 10^6 \text{ t y}^{-1}$ of the Ob and Yenisei rivers is an order of magnitude lower than that for e.g. of the Yukon and MacKenzie rivers (Aagaard and Carmack, 1989; Gordeev et al., 1996) which drain partly glaciated terrain. Most of the terrigenous material supplied by rivers to the Kara Sea is deposited near the river mouths (Lisitzin, 1995). Here, estuaries with their sea water fresh water mixing zone are the link between land and ocean systems and play a special role as potential sinks for riverine sediments (e.g. Dyer, 1986).

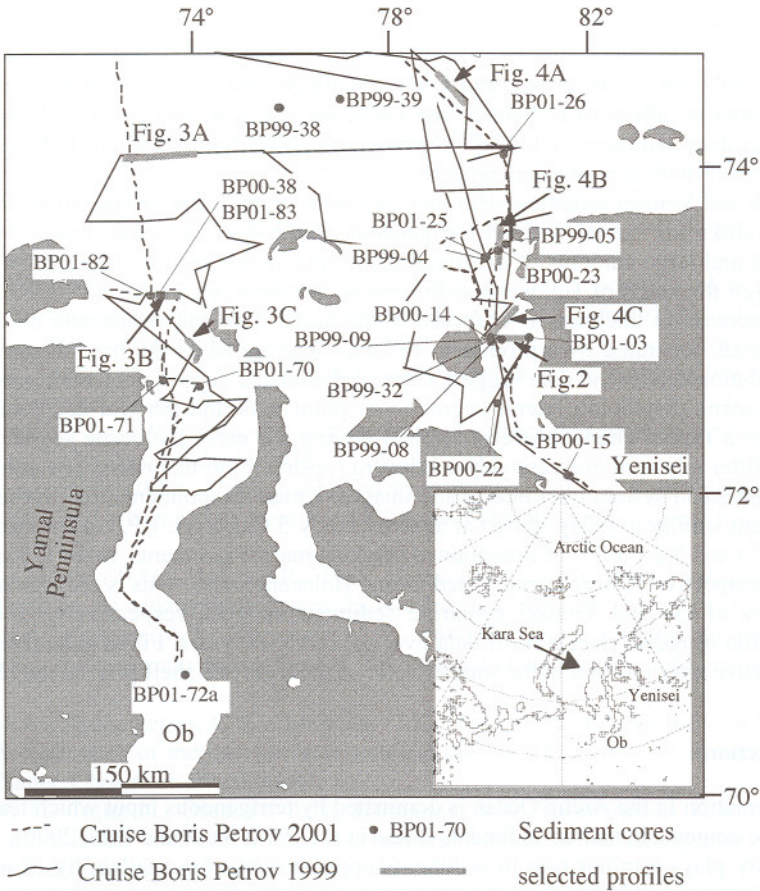


Fig. 1: Location map of working area including track lines of CHIRP/ELAC profiles and core positions. Heavy lines denote positions of profiles shown in Figures 2, 3 and 4.

In the Ob and Yenisei estuaries there are generally two factors controlling sediment accumulation and thus the sediment budget. One is sediment input and the other is erosion and/or resuspension.

Sediment input into the system mainly depends on river run-off which varies strongly both seasonally and interannually (Pavlov and Pfirman, 1995). The annual maximum discharge rate is observed in June. During this peak, 45 to 65% of the annual freshwater run-off and 80% of the annual sediment masses are released (Gordeev et al., 1996; Shiklomanov and Skakalsky, 1994).

In Arctic coastal waters, resuspension and lateral transport of sediments can be enhanced by several factors and processes. These include brine-induced currents associated with sea ice formation (Blanchet et al., 1995; Lisitzin, 1995), wave-induced currents during storm events (Løset et al., 1999; Are, 1996; Stein and Fahl, 2000), sediment erosion by grounding sea ice (Løset et al., 1999; Barnes and Lien, 1987) and incorporation of particles into sea ice during „suspension freezing“ (Reimnitz et al., 1993; Dethleff, 1994). These processes are important on the open shelf with large areas exposed to strong winds and significant sea ice formation. They are not expected to play a major role in sheltered estuaries, such as those of Ob and Yenisei.

Estimations of sediment fluxes on arctic continental margins are rare. Stein and Fahl (2000) quantified the carbon fluxes into the Laptev Sea and Bauch et al. (2000) estimated sediment input in the eastern Laptev Sea shelf. There are some rough flux estimates including the Ob and Yenisei estuaries by Russian authors (e.g. Lisitzin, 1995). Very recently, a synthesis about sediment and organic carbon fluxes in the Arctic Ocean and surrounding marginal seas has been compiled by Stein and Macdonald (2003).

The major aim of this paper is the calculation of a Holocene sediment budget for the estuaries of Ob and Yenisei as a basis for assessment of material fluxes into the Kara Sea and further into the Arctic Ocean. These estuaries may function as major sediment sinks.

In this study, we interpret high-resolution acoustic reflection profiles (2-12 kHz) to map the thickness and lateral extend of fine-grained Holocene sediments between 70° N and 74°30' N (Fig. 1). High-frequency single channel systems are particularly capable to penetrate these muddy sediments. This, in combination with AMS ¹⁴C dating and the physical properties of the retrieved gravity cores, enables us to evaluate the Holocene sediment budget of the area. We further discuss the evolution and depositional history of the Ob and Yenisei estuaries particularly with regard to the post glacial sea-level rise and migration of deposition centers. The data was collected during the expeditions of the RV "Akademik Boris Petrov" in 1999, 2000 and 2001 (Stein and Stepanets, 2000; 2001; 2002; Fig. 1).

In the area of interest extensive surveys have been carried out by Russian authorities and many shallow acoustic lines have been recorded. Unfortunately, this data is not accessible because the region is strategically relevant for military and commercial reasons.

2 Materials and Methods

During three expeditions (1999, 2000 and 2001) more than 5000 kilometers of high-resolution subbottom profiles in the estuaries of Ob and Yenisei were recorded (Fig. 1) using the hull-mounted ELAC system of RV "Akademik Boris Petrov" (ELAC echograph LAZ 72, Honeywell-Nautik, Kiel, Germany) which operates at 12 kHz. In 2001 we amplified and plotted the ELAC signal using a GeoAcoustics receiver and Ultra printer 120, respectively

(Stein and Stephanets, 2002). In addition, for higher acoustic resolution and penetration a towed CHIRP system was used (Geochirp, GeoAcoustics, Great Yarmouth, UK). The CHIRP sweep was set to 2-8 kHz (high-penetration mode). Digitising of acoustic data was achieved with a digital receiver (Octopus 360, Deddington, UK). Analogue data including GPS positions and time were stored on a four-channel DAT recorder. A detailed description of the whole system is given by Stein and Stepanets (2002). Time-to-depth conversion was done using a sound velocity of 1500 m s^{-1} for water (Hamilton, 1972). Digital processing was carried out using PC-based software REFLEX (HarbourDom GmbH, Köln, Germany).

Sediment cores of up to eight meters in length were retrieved with a gravity corer. Whole-core physical properties were measured in 1 cm depth intervals using a Geotek Multi Sensor Core Logger. The system provides data of density, P-wave velocity and magnetic susceptibility (e.g., Schultheiss et al., 1987; Schultheiss and McPhail, 1989; Weaver and Schultheiss, 1990). Changes in these parameters reflect changes in porosity and/or sediment composition (Thompson and Oldfield, 1986; Weber et al., 1997). The technical setup of the logging system, as used during "Akademik Boris Petrov" expedition in 2001, is described in Stein and Stephanets (2002). After splitting the cores were described (Matthiessen and Stepanets, 1999; Stein and Stepanets, 2000; 2001; 2002) and sampled for determination of sedimentological parameters.

For the determination of magnetic susceptibility of surface samples, freeze-dried samples were densely packed in 12.5 cm^3 plastic vials and measured using a MS2B sensor, Bartington Ltd, UK (for further information see Niessen and Weiel, 1996). Mass-specific susceptibility was calculated by normalising volume-specific susceptibility to 10 cm^3 and dividing by the sample weight (Dearing, 1994).

Linear sedimentation rates were calculated between AMS ^{14}C -dated fix points. All AMS ^{14}C ages presented in this paper are in Calendar kilo years B.P. (Cal. kyrs. BP, see Stein et al., this volume). The acoustic subunits were differentiated after the sequence stratigraphy concept of Vail et al. (1977). Mass accumulation rates (MAR) were calculated according to Stein (1991):

$$\text{MAR} (\text{g cm}^{-2} \text{ky}^{-1}) = \text{LSR} * (\text{WBD} - 1.026 \text{ GRP}/100)$$

Sediment porosity was determined by gamma-ray absorption and calculated using the following equation (Weber et al., 1997):

$$\text{GRP} = \frac{\text{Dgp} - \text{GRD}}{\text{Dgp} - \text{Dw}}$$

Where:

GRP = Gamma-ray Porosity

GRD = Gamma-ray Density

Dgp = Grain Density: 2.65 g cm^{-3}

Dw = density of (salt) water: 1.024 g cm^{-3}

LSR = linear sedimentation rate

WBD = wet bulk density

(all values and abbreviations after Weber et al., 1997)

3 Results

3.1 Subbottom profiling and seismic stratigraphy

In general, two major acoustic units (Unit I and Unit II, top to bottom) (Figs. 2 to 4) and three subunits (Ia to Ic; Fig. 2) were distinguished in the echograph profiles. Major units are separated by a distinct reflector (Figs. 2 to 4).

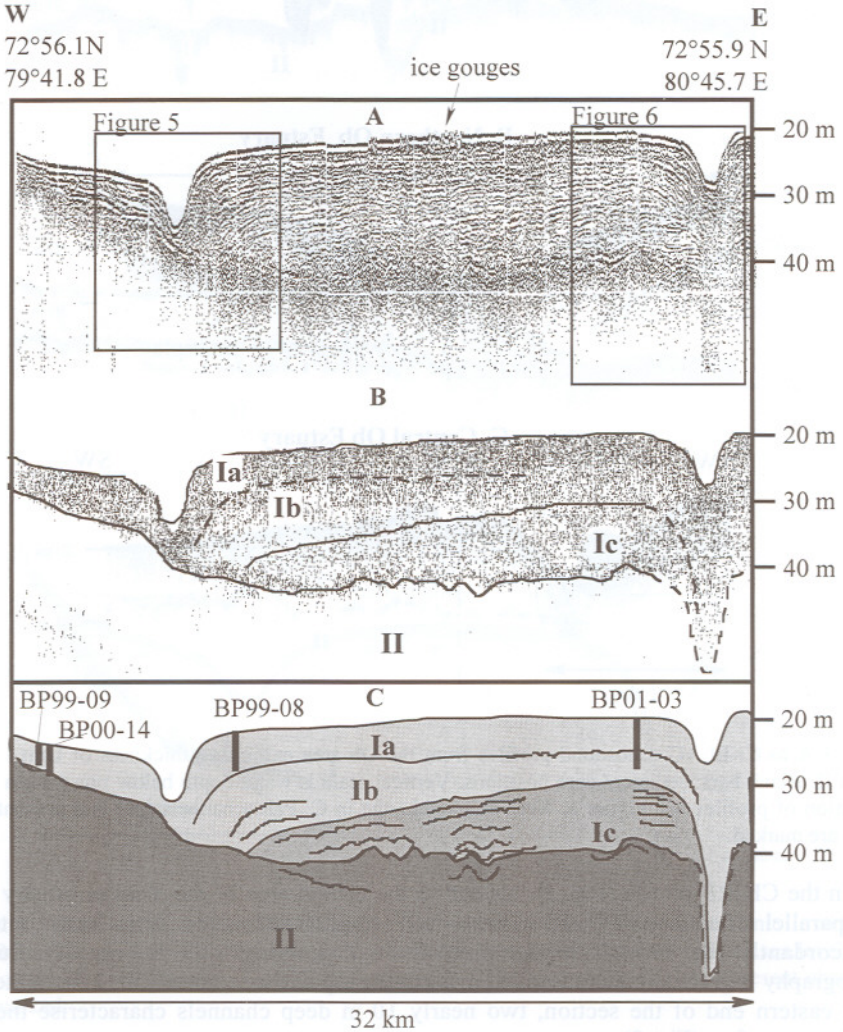


Fig. 2: High-resolution profiles from the central Yenisei Estuary (see Fig. 1 for location). CHIRP (A) and ELAC (B) profiles were recorded simultaneously along the same line. C: acoustic Units and sediment core locations.

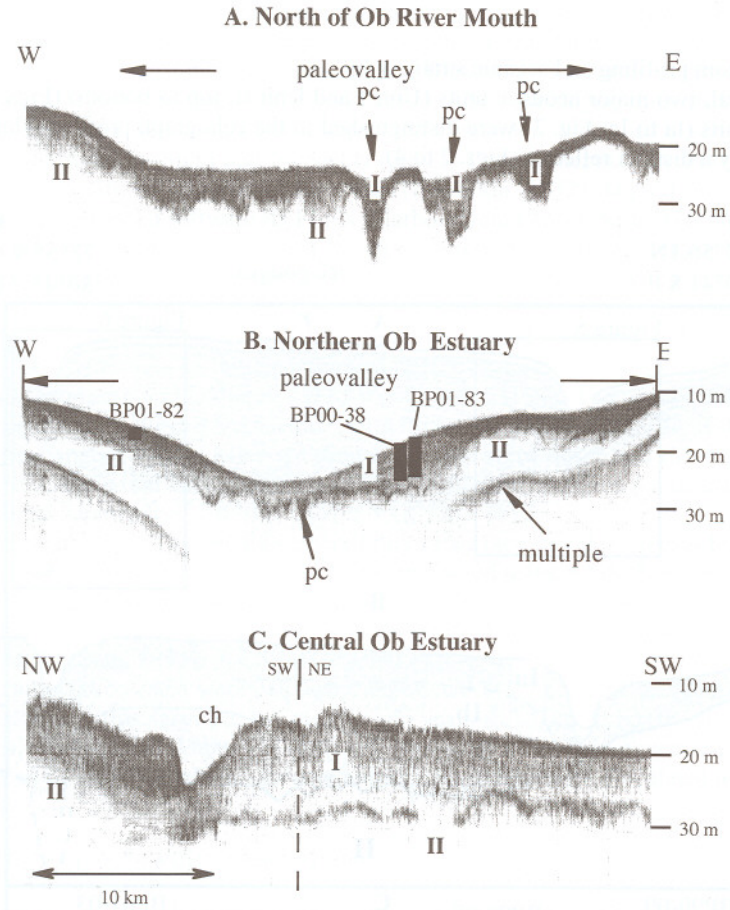


Fig. 3 A to C: ELAC echosound profiles from the Ob area exhibiting thickness of Unit I overlying Unit II. Black bars: sediment core positions. Vertical scale is water depth below present sea level. For location of profiles see Figure 1. Note course change in C. Paleochannels (pc) and present channels (ch) are marked.

In the CHIRP profile (Fig. 2), located in the central area of the Yenisei estuary (Fig. 1), subparallel reflections of Unit I indicate well stratified sediments. At its base Unit I drapes concordantly the variable topography of the underlying Unit II (Fig. 2). Subbottom topography is gradually more levelled towards the top of the sediment fill. In both the western and eastern end of the section, two nearly 10 m deep channels characterise the present sediment surface (Fig. 2).

The CHIRP profile (Fig. 2) and two enlarged profile sections (Figs. 5 and 6) exhibit important detail information about the seismic stratigraphy of Unit I. This record suggests the definition of three subunits Ia to Ic based on their geometries. In general, all subunits of Unit I

are resembling the same back scatter behaviour which is typical of mud (Damuth, 1975; 1978).

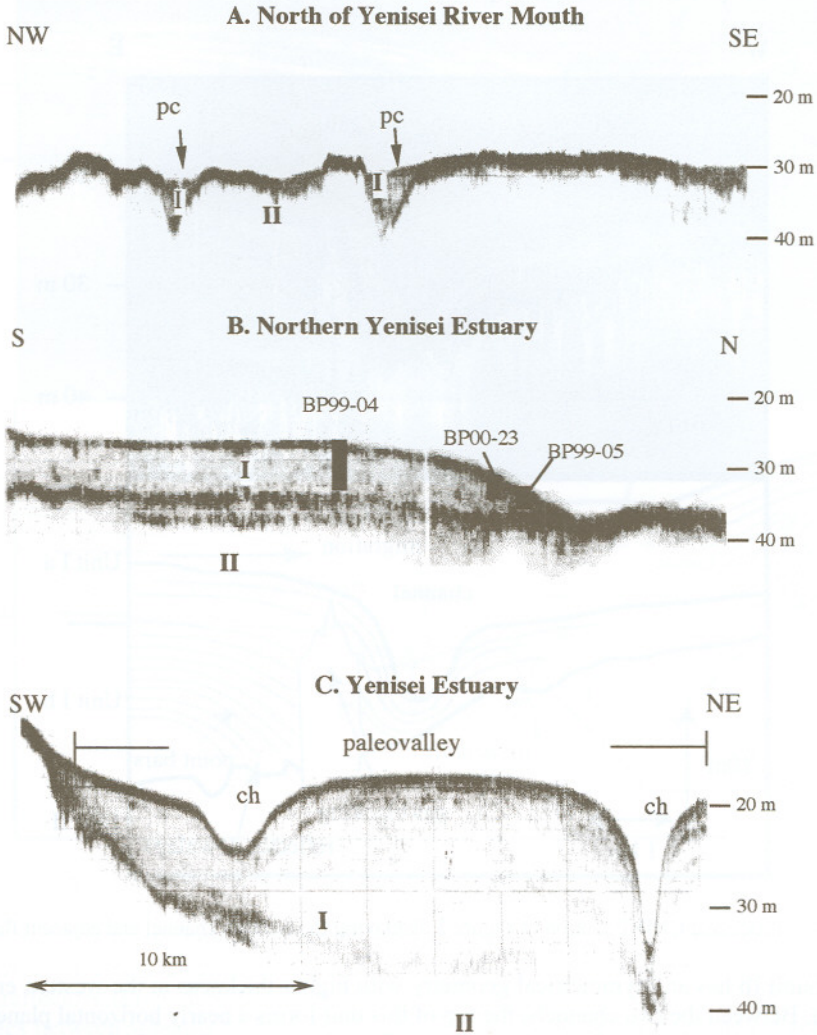


Fig 4 A to C: ELAC echosound profiles from the Yenisei area exhibiting thickness of Unit I overlying Unit II. Black bars: sediment core positions. Vertical scale is water depth below present sea level. For location of profiles see Figure 1. Note course change in C. Paleochannels (pc) and present channels (ch) are marked.

Subunit Ia exhibits almost constant total thickness along the whole profile and very little lateral fluctuations of sediment thickness between individual reflectors including the eastern channel. Only in the western channel some thinning of infill strata can be observed. The

sediment surface exhibits some incision marks typical of ice gouging, especially in the central section of the profile where water depth is 20 m or less (Fig. 2A).

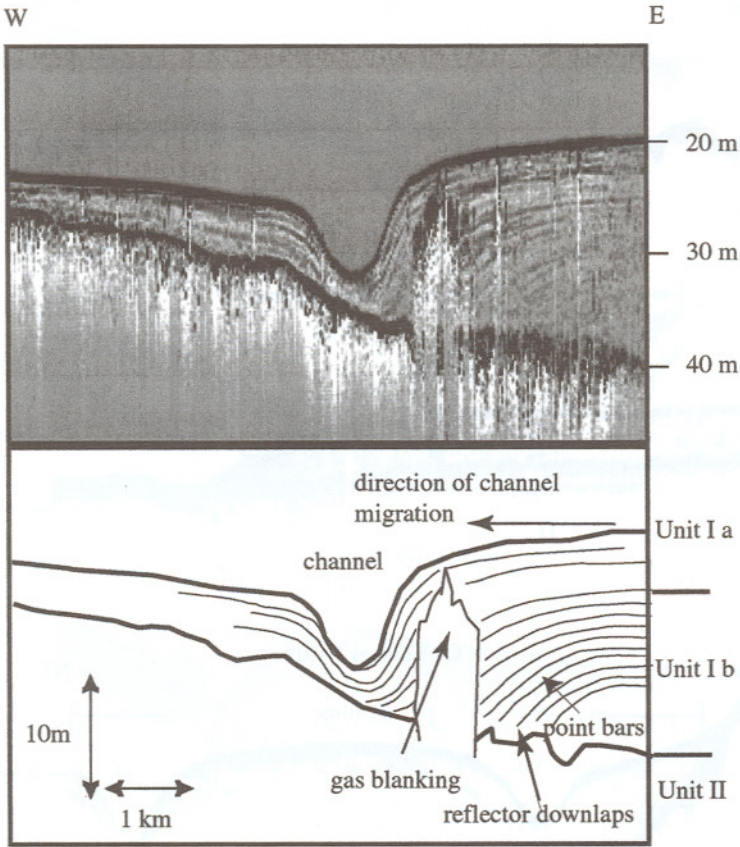


Fig. 5: Processed CHIRP section of Figure 2 displaying the western channel and adjacent flanks.

Subunit Ib has an asymmetrical geometry with higher thickness in the western end of the profile. Between the two channels, the top of this unit forms a nearly horizontal plane at 25 m below present sea level and contains sediment fills of about 5 to 10 m thickness in the eastern channel. In the western area of the CHIRP profile, the asymmetry of Subunit Ib is defined by reflector downlaps onto the surface of Unit II (Figs. 2, 5 and 6). Subunit Ib sediments in the eastern channel are characterised by a complex reflector geometry related to channel migration associated with filling (Fig. 6).

Subunit Ic shows an asymmetrical, prismatic geometry decreasing in thickness to the west with increasing distance from the eastern channel (Fig. 2C). Subunit Ic sediments are missing in both channel locations and towards the outer edges of the profile so that Subunit Ic is only present in the central area of the cross section (Fig. 2C). Near the eastern channel, Subunit Ic sediments exhibit inclined reflector downlaps onto the upper flank of the channel (Fig. 6).

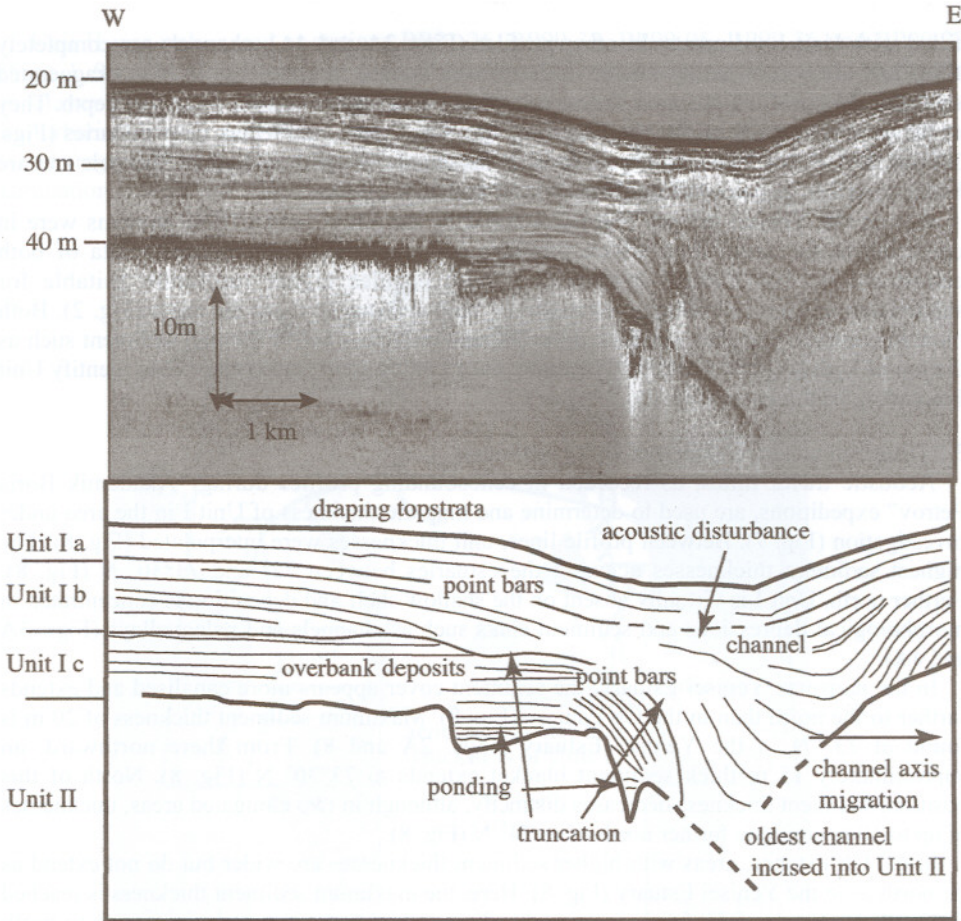


Fig. 6: Processed CHIRP section of Figure 2 displaying the eastern channel and adjacent flanks.

In general, Unit I exhibits the character of a sequence representing a depositional cycle from more asymmetric, channel-levee type of deposits near the base (Ic) to more symmetric type of reflectors (Ia) indicative for sediments draping the cross section at the top. The boundaries between subunits Ia/Ib and Ib/Ic appear to be conformable with the exception of some erosional truncation that is visible near the flank of the eastern channel (Figs. 2 and 6). In places, Unit I is affected by diffractions (Fig. 5) typical of „gas blanking“ (Fader, 1997) which mask the underlying sediments. This may indicate some content of sediment gas possibly related to decomposition of organic matter.

The top of Unit II forms a prominent reflector which is present in the whole working area both in CHIRP and ELAC profiles (Figs. 2 to 4). The acoustic impedance contrast between Unit I and Unit II appears to be large because there is almost no penetration below. The surface of Unit II shows an irregular, rough morphology indicative of an erosional surface. Paleochannels incised into Unit II including the eastern channel of the CHIRP profile (Figs. 2A and 6) and several channels recorded in ELAC profiles (Figs. 3C and 4C) which are partly

filled with Unit I sediments. In other profiles (Figs. 3A and 4A), channels are completely filled and are not, or hardly visible in the present surface morphology. In high exaggerated echosounding profiles, channels appear as typical v-shaped incisions of 5 to 10 m depth. They occur more frequently on the shelf north of 73°N in front of the recent river estuaries (Figs. 3A and 4A). Some incisions appear to be considerably wider than distinct channels and are better described as paleovalleys (Figs. 3A, 3B and 4C).

Across the Yenisei estuary (Figs. 2A and 2B), the ELAC and CHIRP systems were in operation at the same time which provides a direct comparison between data of both echosounders. The CHIRP system (2-8 kHz) enables higher resolution suitable for subdivision of Unit I although penetration of both systems is about the same (Fig. 2). Both have in common that they can pick up prominent reflectors below the soft sediment such as the top of Unit II (Figs. 3 and 4). Therefore, the ELAC system is also capable to identify Unit I including its thickness (Fig. 2).

3.2 Distribution and thickness of Unit I sediments

Acoustic travel times, as recorded in echosounding profiles during "Akademik Boris Petrov" expeditions, are used to determine and map the thickness of Unit I in the area under investigation (Fig. 7). Between profile lines, unit thicknesses were interpolated (Fig. 8). The highest sediment thicknesses occur in the estuaries between 72° and 73°30' N (Fig. 8). Further north, Unit I is virtually absent on the shallow shelf and deposition is concentrated in morphological depressions and sediment sinks such as channels and paleovalleys (Figs. 3A and 4A).

In the narrower Yenisei Estuary, the sediment cover appears more canalised and extends further to the north than in the Ob Estuary (Fig. 8). Maximum sediment thickness of 20 m is found at 73° N in the Yenisei Estuary (Figs. 2A and 8). From there northward, an approximately 15 m thick sediment blanket extends to 73°30' N (Fig. 8). North of this position, sediment thickness decreases distinctly, although in two elongated areas, thicknesses of up to 10 m continue further north up to 74° N (Fig. 8).

In the Ob Estuary, areas with higher sediment thicknesses are wider but do not extend as far north as in the Yenisei Estuary (Fig. 8). Here, the maximum sediment thickness is reached at 72°20' N. North of 72°50' N increased sediment thickness occurs along a south to north directing axis following 73° E. There is a second area with lower sediment thickness of up to 10 m extending in a SW-NE direction near 74° E.

3.3 Sediment-core lithology, physical properties and chronology

According to the lithological descriptions of the cores from the area under investigation (Stein and Stepanets, 2000; Stein et al., this volume), major changes in lithology correspond with both boundaries between acoustic units (Fig. 9) and distinct changes in physical property records (Figs. 10 to 12).

Lithological descriptions of sediment units

The predominant lithology of Unit I is a clayey silt to silty clay (Stein et al., this volume) with quartz and clay minerals as major components (e.g. Stein and Stepanets, 2000). Bivalve shells associated with bioturbation are very common which can grade into horizontal, non-bioturbated bedding with fewer shells in the lower sections of Unit I (e.g. Stein and Stepanets, 2000).

Unit II was only cored at stations BP01-26, BP99-38, BP99-05, BP99-36 and BP00-22 (Figs. 1, 9 to 12). Unit II exhibits generally coarser sediments ranging from sandy clayey silt to clayey silty sand (Stein et al., this volume). Unit II is mostly unfossiliferous and bioturbation is very rare (Stein and Stepanets, 2000). Occasionally plant debris occurs as wood fragments, but aquatic fossil fragments like mollusc shells are absent. Often, distinct lamination is observed which is disrupted by some erosional contacts.

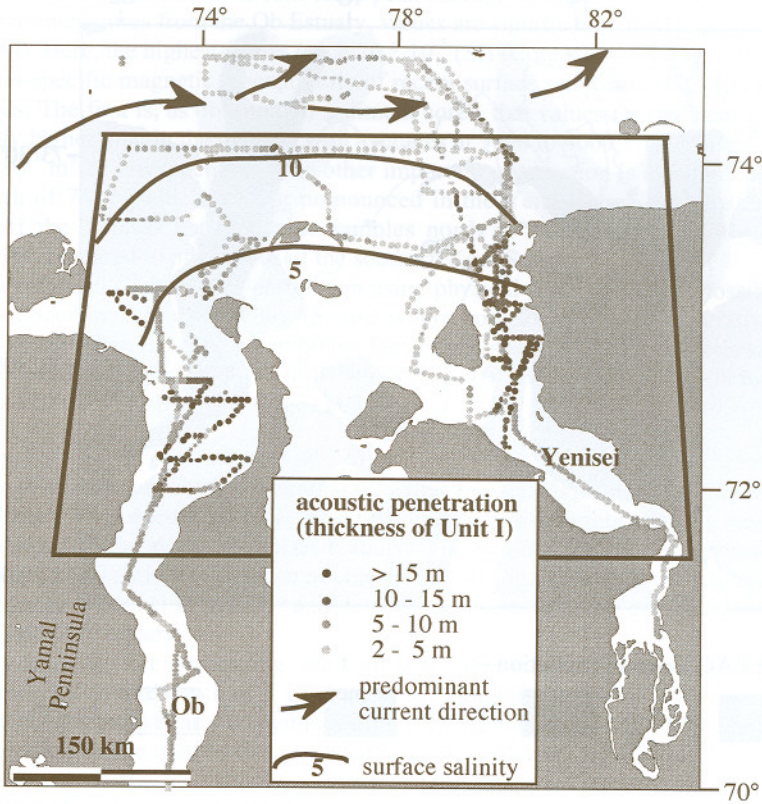


Fig. 7: Data base of thickness quantification of Unit I by determination of acoustic penetration along ELAC/CHIRP profiles. Current direction and surface salinity after Pavlov and Pfirmann (1995). The trapeze indicates position of Figure 8.

Physical properties

Density and Porosity: Whole-core wet bulk density generally increases with core depth (Figs. 10 to 12). Wet bulk density ranges from 1.3 g cm^{-3} to 2.3 g cm^{-3} with a mean of 1.57 g cm^{-3} for all measured values. On average, the density values of Unit II are 0.4 g cm^{-3} higher than in Unit I. In most cores, the transition from Unit I to Unit II is characterised by a steep gradient with peak densities at or near the top of Unit II (Figs. 10 to 12).

After calculating porosity from density data of all cores (Figs. 10 to 12), an average porosity of Unit I sediments of 66% was quantified for all stations (Fig. 1). This porosity is used to determine the bulk net sediment mass from the sediment volume of Unit I (Figs. 7 and 8; Table 1) determined by sediment echosounding (see 3.4).

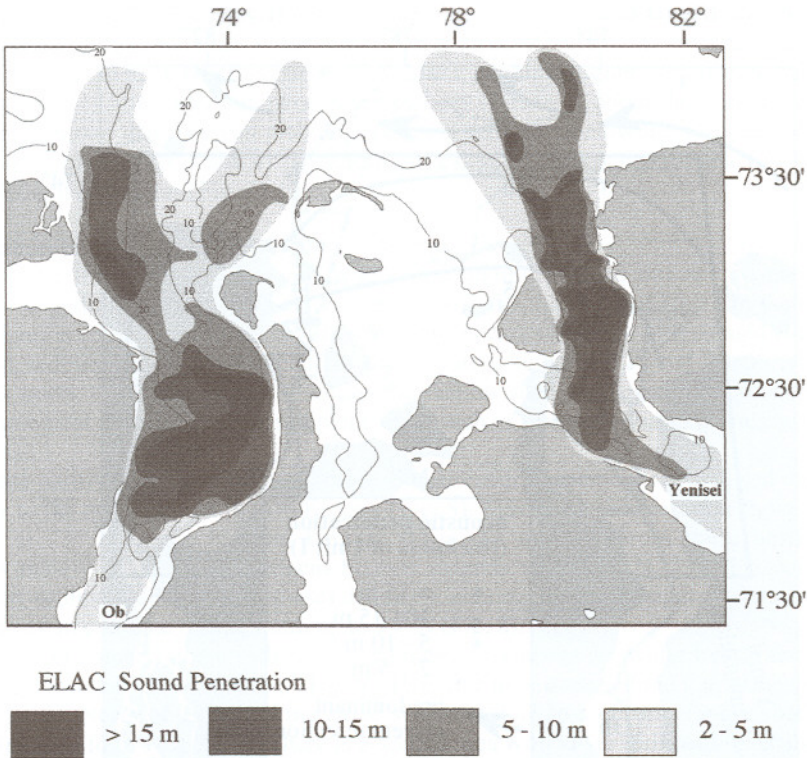


Fig. 8: Isopach map showing the total thickness and extend of acoustic Unit I in Ob and Yenisei estuaries based on ELAC/CHIRP profiles. Water depth in meters.

Magnetic Susceptibility: In general, the upper part of Unit I displays the lowest susceptibilities gradually increasing down-core (Figs. 10 to 12). Similar to the density records, the transition from Unit I into Unit II is often characterised by a steep gradient with peak susceptibility at the boundary between Unit I and Unit II (Figs. 10 to 11) cores BP99-04, BP99-09, BP00-23 from the Yenisei and BP00-38, BP01-83 from the Ob estuaries (Fig. 12). In some cores higher susceptibility values are associated with increased density as, for example, in cores BP99-32, BP01-03 (Fig. 11), BP01-83 and BP00-38 (Fig. 12). These values can probably be accounted to decreased sediment porosity and thus more susceptibility

bearing material in the core rather than a change in dry sediment composition. Other cores show susceptibility fluctuations independent of the density record as, for example, in cores BP99-39, BP99-04, BP00-23, BP00-14 (Fig. 10) and BP00-22 (Fig. 11) indicative for variations in content and/or composition of magnetic grains.

In the Yenisei Estuary, susceptibility is $100 \cdot 10^{-5}$ (SI) on average with peak values of $250 \cdot 10^{-5}$ (SI) and $550 \cdot 10^{-5}$ (SI) in core BP00-22 and BP00-23, respectively (Figs. 10 and 11). Both cores penetrate Unit II and in both cores peak susceptibility values are in Unit II (Figs. 9 to 11). In sediment cores from the Ob Estuary, values are significantly lower, averaging about $30 \cdot 10^{-5}$ (SI). Here, the highest values reach $70 \cdot 10^{-5}$ (SI) (Core BP00-38; Fig. 12).

The mass-specific magnetic susceptibility of recent surface sediments (Fig. 13) shows two major trends. The first is, as observed in sediment cores, that values for the Yenisei river are significantly higher than in the Ob area with averages at 3000 to $4000 \cdot 10^{-9} \text{ m}^3 \text{ kg}^{-1}$ and 1000 to $1500 \cdot 10^{-9} \text{ m}^3 \text{ kg}^{-1}$, respectively. The other important observation is a distinct decrease in values north of 74° N which is most pronounced in the Yenisei area. Despite the distinct decrease off the Yenisei Estuary some samples north of 74° N show slightly increased susceptibility compared to other areas of the southern Kara Sea.

Core correlation: Core-to-core correlation using physical properties is not possible for the entire area under investigation. Only in case where core locations are in relatively close distances to each other, lateral correlation by density and susceptibility is obvious such as for cores BP99-04 to BP01-25, BP99-39 to BP99-38 (Fig. 10), BP99-32 to BP99-08 to BP01-03 (Fig. 11) and BP00-38 to BP01-83 (Fig. 12).

Chronology

All datings of sediment cores penetrating into Unit I reveal Holocene ages (Fig. 9, Stein et al. this volume). The oldest Unit I age of 9 Cal. kyrs. BP is determined at the base of Core BP99-04 located in the norther Yenisei Estuary. The distinct down-core increase of both density and susceptibility at the bottom of core BP99-04 (Fig. 10) suggests that the transition into the underlying Unit II is exposed and dated and the gravity corer got stuck at or shortly above the Unit I/II boundary.

The only dateable core penetrating into Unit II is BP99-05. An age of 15.5 Cal. kyrs. BP was determined at a core depth of 3.15 m (Fig. 9). The dated material is a relatively fresh shrub wood suggesting a nearly contemporaneous sedimentation. Though it is driftwood, the good preservation can be used as first evidence for a pre-Holocene age of Unit II.

3.4 Correlation of acoustic units with sediment cores

The coring locations BP00-14, BP99-32, BP99-08 and BP01-03 are on the track of the CHIRP profile (Fig. 2C). BP00-14 cored both Unit I and II. Lithology and physical properties demonstrate that the increase in sand content correlates with higher density. The density gradient defines the major acoustic impedance contrast causing the strong seismic reflector at the boundary between Units I and II. The same is true for a correlation of Unit I/II boundaries cored by BP00-23 and BP99-05 (Fig. 9) with the ELAC profile from the northern Yenisei Estuary (Fig. 4B). This suggests that the transition from Unit I to II observed in cores and acoustic profiles are identical in the entire area.

The only core, which clearly penetrated the acoustic boundary between subunits Ia and Ib of the CHIRP profile, is BP01-03 whereas BP99-32 and BP99-08 probably only comprise Subunit Ia sediments (Fig. 2C). The boundary between Subunit Ia and Ib is insignificant in

physical property records of both density and susceptibility (Figs. 10 to 12) and not visible in the lithology (Fig. 9).

Along the CHIRP profile, Subunit Ic was not cored because it is below the maximum gravity-corer sediment-penetration limit of about eight meters (Fig. 2C).

Along ELAC profiles, where cores recovered both Unit I and Unit II sediments, Subunit Ic could not be identified due to limited echosounding resolution or may not be present.

3.5 Sediment mass

The total sediment volume was calculated from the areal extend of Unit I sediments, compiled by echosounding, multiplied by its thickness (Figs. 7 and 8; Table 1). The amount of dry sediment was quantified by subtracting the average volume of pore water (66% porosity) from the total wet sediment volume. The net sediment mass was then quantified by multiplying the porosity corrected value of dry sediment volume with the average grain density of 2.65 g cm^{-3} (e.g. Weber et al., 1997).

The total estimated sediment yields of the estuaries of Ob and Yenisei differ significantly but are in the same order of magnitude (Table 1). Acoustic Unit I yields $14.3 * 10^{10} \text{ t}$ and $9.2 * 10^{10} \text{ t}$ of dry sediment (Table 1) in the Ob and Yenisei estuaries, respectively.

Table 1. Quantified sediment area and volume based on isopach map (Fig.8). The net sediment mass was determined by the sediment volume and the average porosity of sediment cores and the average dry grain density.

Sediment Thickness (m)	Area (km^2)	Volume (km^3)	Netto Sediment Mass (* 10^{10} t)
Yenisei			
>15	1815.1	31.8	
<15	2022.1	25.3	
<10	3789.4	28.4	
<5	6512.1	19.5	
total		105.0	9.2
Ob			
>15	2452.0	42.9	
<15	3805.4	47.6	
<10	5938.9	44.5	
<5	8709.4	26.1	
total		161.1	14.3

4 Discussion

4.1 Late Quaternary sedimentary environments

Age model

The radiocarbon datings of Unit I and II suggest that the boundary may represent the pre-Holocene transition or unconformity. The susceptibility spike observed near the top of Unit II in cores BP99-05, BP99-09, BP99-38, BP00-23 and BP00-22 (Figs. 9 and 10) is similar to a comparatively high spike of susceptibility described in cores from the eastern Kara Sea and Laptev Sea by Kleiber and Niessen (2000).

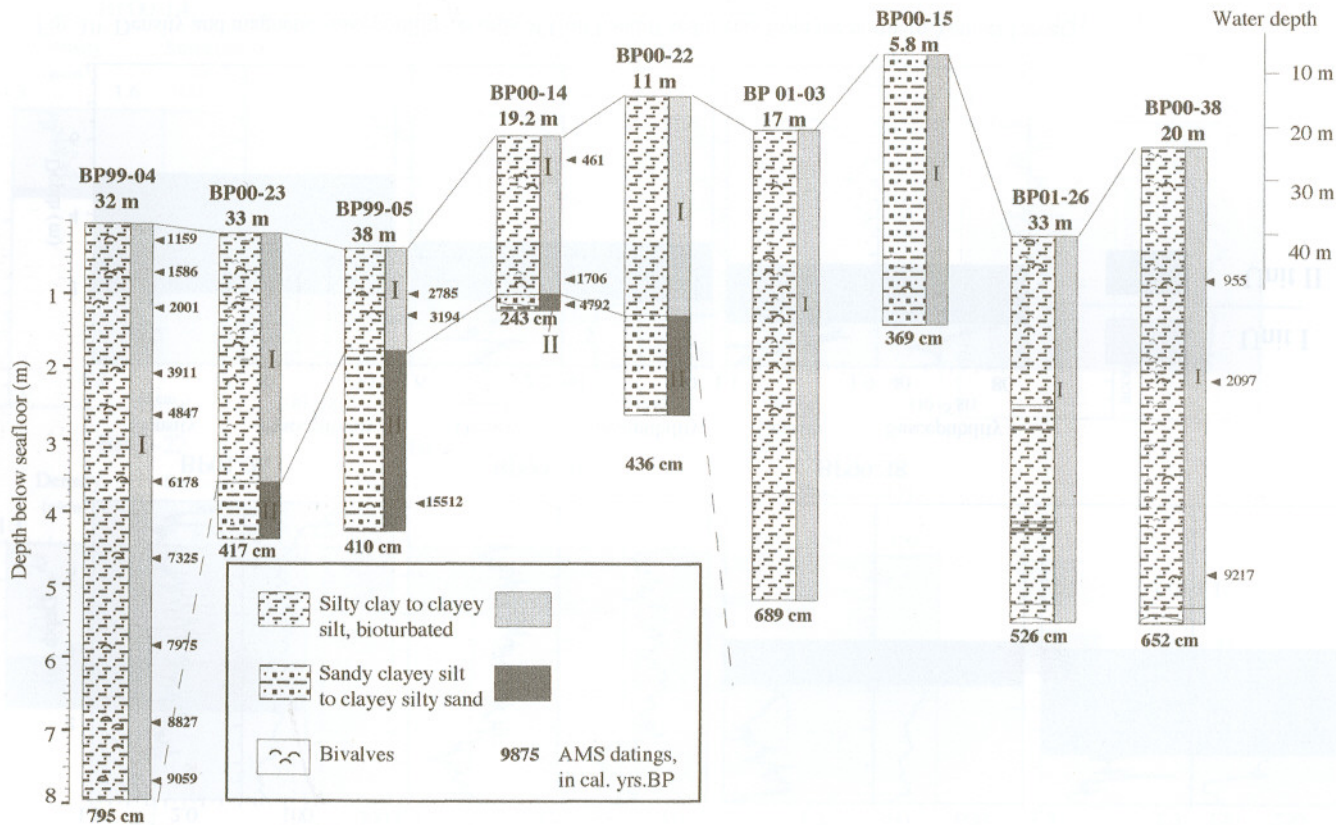


Fig. 9: Stratigraphic correlation of selected cores based upon core description and datings. Cores are arranged according to water depth (right hand scale). See Figure 1 for location.

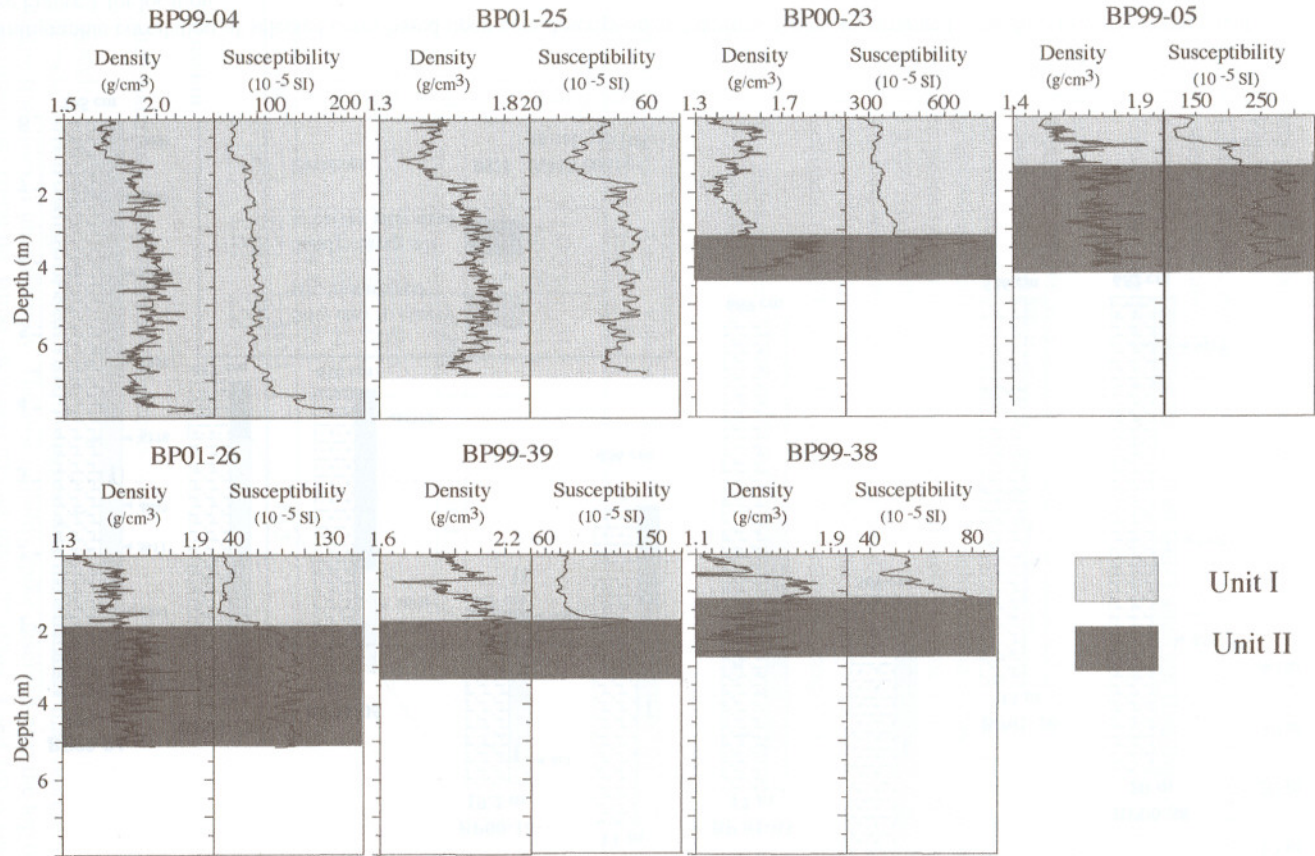


Fig. 10: Density and magnetic susceptibility records of Unit I and II sediments from the northern Yenisei Estuary.

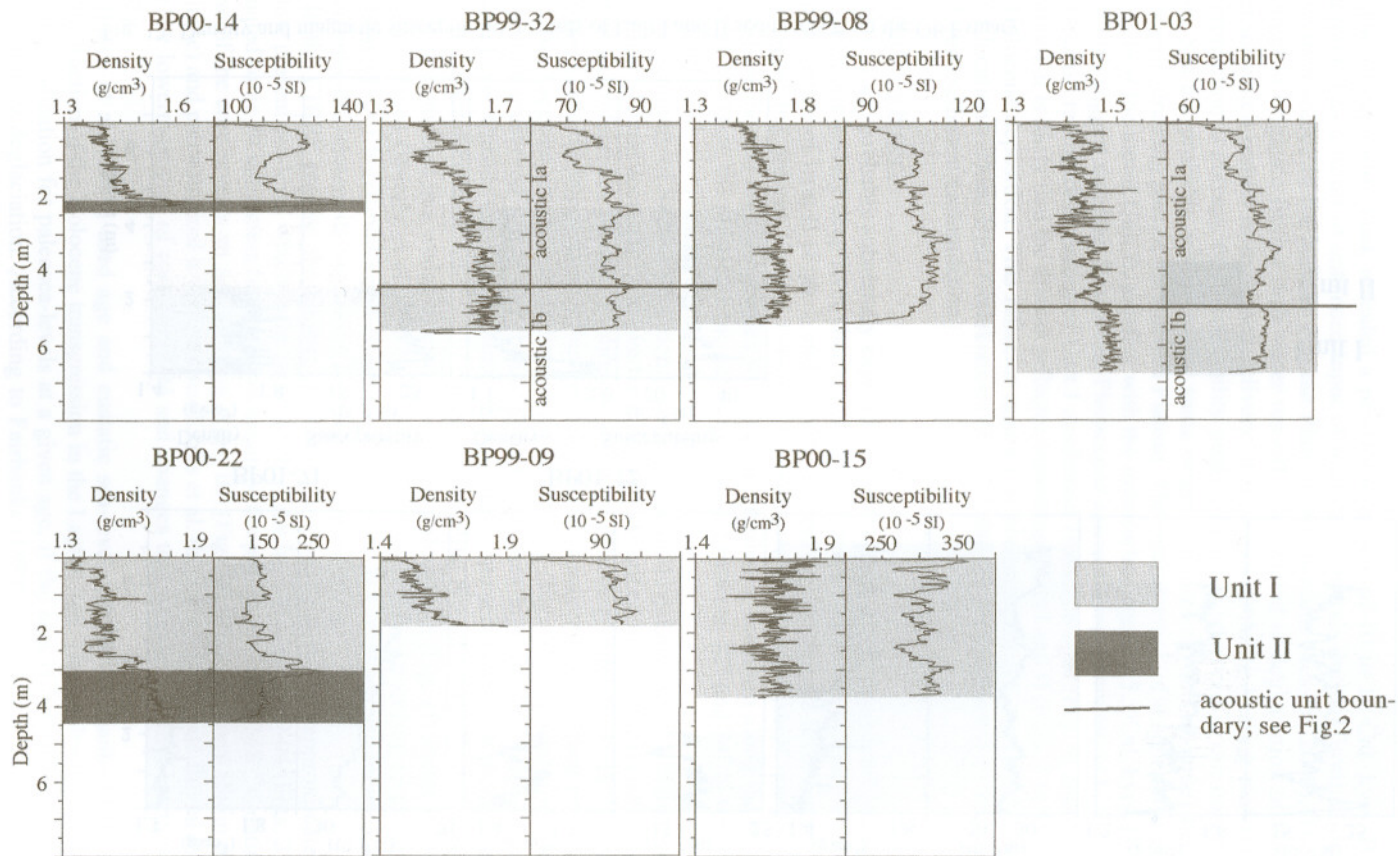


Fig. 11: Density and magnetic susceptibility records of Unit I and II sediments from the central Yenisei Estuary.

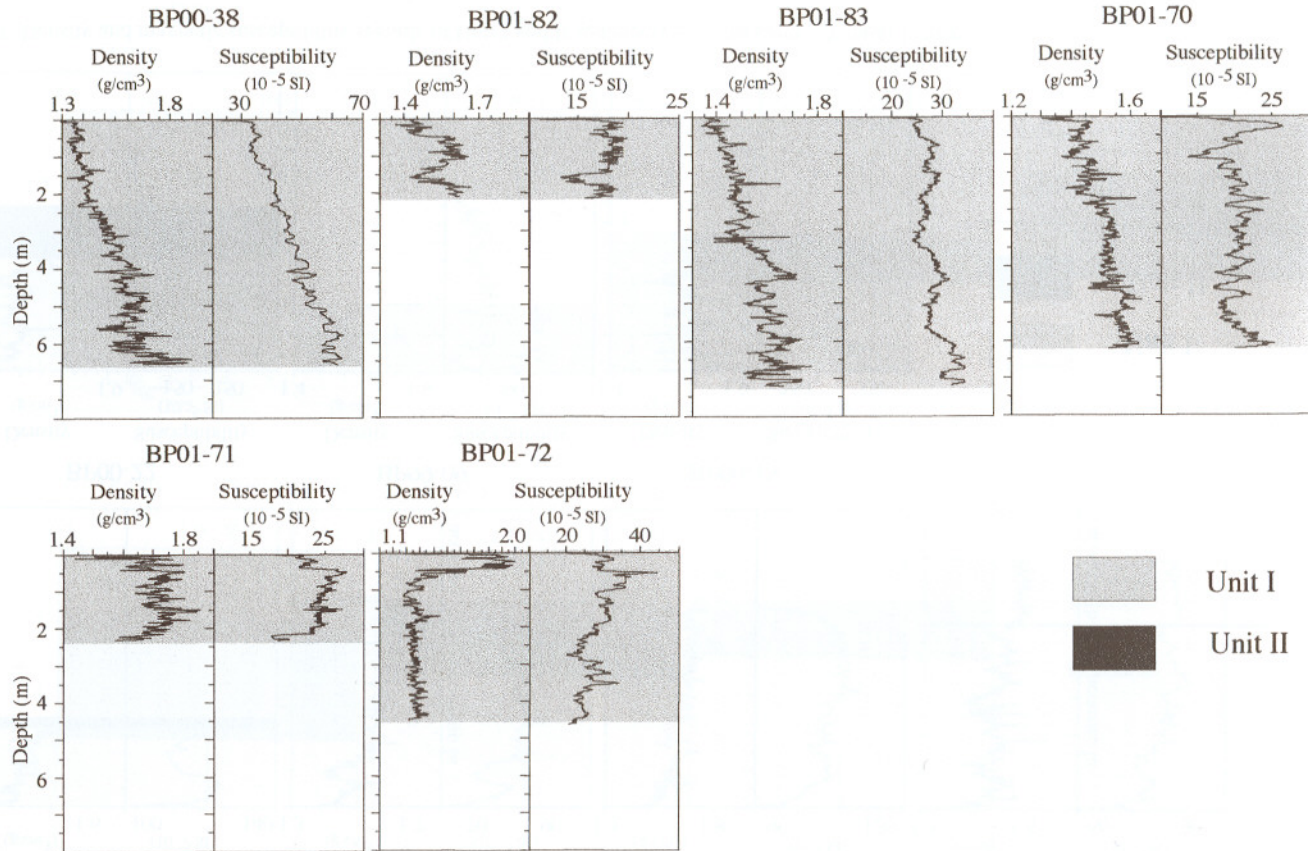


Fig. 12: Density and magnetic susceptibility records of Unit I and II sediments from the Ob Estuary.

The susceptibility peak revealed a pre-Holocene age of 10 to 13 Cal. kyrs. BP and is interpreted as a result of enhanced input of magnetic minerals during Termination I which have their source in the basaltic Putoran Plateau (Kleiber and Niessen, 2000). The spike is thought to originate from a melt water run-off peak related to deglaciation of the Putoran Plateau which results in increased delivery of high susceptibility bearing material. If this interpretation is correct, the susceptibility peaks of Unit II observed in our cores from the Kara Sea are probably related to the same origin (Stein et al., this volume) because the Yenisei is draining part of the Putoran Plateau. The interpretation of magnetic susceptibility peaks near the top of Unit II, together with the radiocarbon age of 15.5 Cal. kyrs. BP of Core BP99-05, suggest that Unit II is of late Pleistocene age including Termination I.

Because radiocarbon dating of Unit I confirmed Holocene ages (Fig. 9; Stein et al., this volume), it is likely that the distinct reflector separating Units I and II (Figs. 2 to 4) is the base of Holocene deposition. This reflector appears as pre-transgressive, erosional boundary in most locations. Thus, Unit I thicknesses (Figs. 7 and 8) are interpreted to represent total Holocene sediment accumulation.

Sedimentary history

Unit II was probably subaerially exposed and partly eroded during sea-level low stand. For example, a relatively deep river channel (at least 55 m below present sea level) was incised into the strata of Unit II (Figs. 2 and 15: Phase I) during the last sea-level lowstand at the location of the present Yenisei Estuary. According to the modern shelf morphology, the paleoshoreline and related estuaries were situated further to the north along the present day outer shelf. Thus, the pre-Holocene paleoenvironment between 72° and 74° N was fluvial or subaerially with erosion as predominant process.

The geometry of Subunit Ic is dominated by typical fluvial architecture elements such as point bars (lateral accretion) and overbank deposits described by e.g. Allen (1965) and Miall (1996 and references therein) in modern fluvial sedimentary environments. In Subunit Ic downlaps onto the upper channel flank are interpreted as accretion of inclined point bars (Fig. 6). This suggests channel migration towards the east (Fig. 6). There are no Subunit Ic sediments preserved inside the channel which indicates high current velocities near the channel axis. Outside the channel, strata grade laterally into sediments with parallel reflectors. This indicates decreased influence of currents resembling typical overbank sediments (Allen, 1965), accumulated in a wedge-shaped structure on a floodplain (Fig. 15: Phase II), typical of a natural levee (Brierly et al., 1997; Bown and Kraus, 1987). According to Galloway and Hobday (1996) horizontal aggradation on a floodplain occurs when sediment-laden water overflows and releases its suspension load due to flow stripping.

In the CHIRP profile, the bottom of Subunit Ic (Fig. 2) is located approximately 40 m below present sea-level which is the same depth as the base of core BP99-04 (Figs. 2 and 4B) situated some 80 kilometers further downstream of the profile (Fig. 1). AMS ¹⁴C dating of the base of the core reveals an age of 9 Cal. kyrs. BP (Fig. 9). Sedimentology (Stein et al. this volume) and palynological investigations (Kraus et al. this volume) indicate fluvial influences for the lowermost part of core BP99-04 and changes to a marine environment in the upper part.

Bauch et al. (2001) used age and eustatic sea-level data by Fairbanks (1989) for the reconstruction of the Holocene transgression in the Laptev Sea. The sea-level curve serves as a rough indication for paleosea-levels at a given age, if the area is not affected by isostatic rebound after deglaciation. According to Fairbanks (1989) the eustatic sea-level trend was

about 30 m below present at 9 Cal. kyrs. BP (Fig. 14). Assuming no (or negligible) isostatic rebound of the Yenisei Estuary area during the Holocene, the onset of sedimentation in core BP99-04 took place near the sea level in very shallow water (Fig. 14). If true both locations BP99-04 and the CHIRP profile (Fig. 1) must have been strongly influenced by the palaeoriver Yenisei at 9 Cal. kyrs. BP. This is consistent with the fluvial character of the lowermost sediments of Core BP99-04 and the interpretation of the seismic pattern above. This suggests a terrestrial, fluvial dominated depositional environment for Subunit Ic in the CHIRP profile (Fig. 2). The paleoenvironment of Subunit Ic is best explained by a fine-grained meandering river system as proposed e.g. by Miall (1996). Probably, pronounced seasonal flood events similar to those observed in Siberian rivers today during late spring/early summer (Gordeev et al., 1996; Shiklomanov and Skakalsky, 1994) caused the accumulation of overbank deposits on the floodplain.

The age of the boundary between subunits Ib and Ic is difficult to assess because the core, which penetrated this boundary, is not dated yet (Fig. 9). However, the truncations at the top of Subunit Ic in Figure 6 could originate from an erosional transgressional ravinement surface (Thorne and Swift, 1991). This surface possibly formed in response to the landward migration of the shoreline associated with erosion during transgression, for example, as a result of wave action. If the entire Subunit Ic is a relict fluvial floodplain deposit, the marine transgression reached the top of this unit (30 m below present sea level, Fig. 2) at about 8.5 to 8 Cal. kyrs. BP (Fig. 14) and formed the onset of marine/estuarine Subunit Ib.

Subunit Ib is characterised by sediment accumulation in the entire channel with highest bed thickness at the channel axis that thins towards the flanks resulting in a divergent fill geometry (Fig. 6; Mitchum et al., 1977). This suggests a gradual decrease in current velocity possibly related to increasing water depth during an early Holocene transgression associated with higher settling rates of particles in a shallow and widening estuarine environment.

As a result of rapid sedimentation in the eastern channel, the upper portion of Subunit Ib reached a higher bathymetric level than the channel base at the western end of the profile where no Subunit Ic and Ib sediments accumulated (Fig. 2). Subsequently, near the western deepest point of the profile, a new channel system was established, where point bar deposits migrated westward forming Subunit Ib downlaps onto Unit II (Fig. 5). Formation of the western channel (Fig. 5) started in the same range of water depth (downlaps on Unit II at approx. 35 to 40 m below sea level; Fig. 2) as the termination of current controlled sedimentation in the eastern channel (Fig. 6). The western channel displays sediment layers that are thinner at the channel base than at the adjacent flanks (Fig. 5) which is typical of an aggradating channel-levee-complex (Allen, 1965). The western channel probably represents the recent thalweg because, at present, its channel bottom has the maximum water depth of the entire cross section (Fig. 2C). In addition, the slightly thinner channel fill suggests that recent sedimentation is affected by currents.

The entire Subunit Ib is typical for a shallow marine/estuarine channel-levee-complex characterised by high sedimentation rates in both channel and levee areas. The change in the depositional environment compared to Subunit Ic is interpreted as the result of sea-level rise, decrease in current velocity and southward migration of marginal filter-type deposition centers. It is interesting to note that the well defined chronology of Core BP99-04, located 80 km to the north of the CHIRP profile also revealed high sedimentation rates for the early Holocene until about 7.5 Cal. kyrs. BP which gradually decrease to lower rates until about 5 Cal. kyrs. BP (Fig. 9). Consistently high sediment accumulation rates of 650, 250, and 240 (g

$\text{cm}^2 \text{ky}^{-1}$) are quantified between 9.5 to 7.5 Cal. kyrs. BP in cores BP00-36, BP00-26, and BP00-07 located 390 km, 250 km, and 130 km north of the Yenisei Estuary, respectively (Stein et al. this volume). It is suggested that these early Holocene deposition centers north of the present estuaries are lateral counterparts of the rapidly filling shallow-marine channel-levee-systems of Subunit Ib indicative of a southward migration of the marginal filter during the transgression.

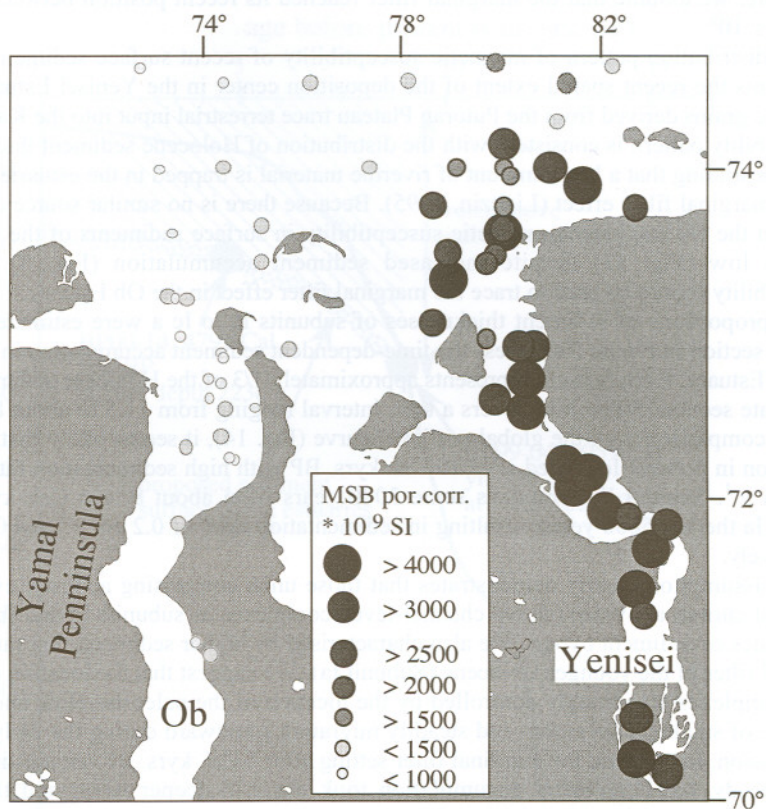


Fig. 13: Mass-specific magnetic susceptibility of surface sediments in the Ob and Yenisei estuaries and the adjacent inner Kara Sea.

Draping subbottom topography and nearly constant thickness of Subunit Ia implies precipitation-type of particle settling out of the water column across the entire estuary, possibly overprinted by more active bottom currents in the western channel. This pattern is typical for the marginal filter setting of today with a relatively stable high sea level where salinity induced processes are important such as particle coagulation followed by rapid settling. Retrieved near the western end of the CHIRP profile from 19.2 m water depth, core BP00-14 reveals a minimum age of 4.8 Cal. kyrs. BP for the base of Subunit Ia (Fig. 9). This

suggests a major hiatus at the core location with Subunit Ia unconformably overlying Unit II. This is consistent with the seismic stratigraphy (Fig. 2) indicating that subunits Ib and Ic are missing at the coring location. The hiatus was possibly caused by subaerial exposure during the early Holocene until the transgression reached the location.

It seems to be reasonable that the onset of the drape geometry of Subunit Ia is related to the end of the transgression which reached the present sea level by about 5 Cal. kyrs. BP. Therefore, we assume that the marginal filter reached its recent position between 7.5 and 5 Cal. kyrs. BP.

The distribution pattern of magnetic susceptibility of recent surface sediments (Fig. 13) documents the recent spatial extent of the deposition center in the Yenisei Estuary because magnetic grains derived from the Putoran Plateau trace terrestrial input into the Kara Sea. The susceptibility pattern is consistent with the distribution of Holocene sediment thickness (Fig. 8) demonstrating that a large amount of riverine material is trapped in the estuaries indicative for the marginal filter effect (Lisitzin, 1995). Because there is no similar source of magnetic grains in the Ob catchment, magnetic susceptibility in surface sediments of the Ob Estuary remains low (Fig. 13) despite increased sediment accumulation (Fig. 8). Therefore susceptibility cannot be used to trace the marginal filter effect in the Ob Estuary.

The proportions of sediment thicknesses of subunits Ia to Ic were estimated from the transect section in Figure 2 to assess the time-dependent sediment accumulation in the present Yenisei Estuary. Each Subunit represents approximately 1/3 of the Holocene sediments in this particulate section. Subunit Ic covers a time interval ranging from 11.5 to about 8 Cal. kyrs. BP. By comparison with the global sea level curve (Fig. 14), it seems likely that significant deposition in Subunit Ic started after 10 Cal. kyrs. BP with high sedimentation rates of about 0.33 cm y^{-1} . Subunit Ib comprises some 3000 years from about 8 to 5 Cal. kys. BP and Subunit Ia the last 5000 years, resulting in sedimentation rates of 0.2 cm y^{-1} and 0.14 cm y^{-1} , respectively.

This assumption clearly demonstrates that those units comprising acoustic evidence for enhanced current activities (active channel-levee-complexes as subunits Ia and Ib), and thus higher rates of sediment bypass, are also characterised by higher sedimentation rates than the marginal filter of the younger Holocene (Subunit Ia). We suggest that the location of channel-levee-complexes are strongly controlled by the location of the paleoshoreline and sea level, therefore of small spatial extent and steadily migrating southward during the early Holocene transgression. In contrast, the marginal filter setting after 5 Cal. kyrs. BP remains in relatively stable steady state. Sediment accumulation took place in deeper water and thus over a relatively large area (Figs. 2 and 8) resulting in overall lower sedimentation rates.

4. 2 Sediment budget

The Holocene sediment budget from seismic data and sediment cores as presented in this paper is difficult to test because a number of uncertainties remain which affect the sediment accumulation. This includes additional input from coastal erosion long-term variations in the riverine discharge, and transfer rates from the estuaries to the shelf. The effect of these processes are hard to quantify with an appropriate spatial and temporal resolution.

For example, Rachold et al. (2003) conclude for the Laptev Sea that the amount of coastal erosion ($44 * 10^6 \text{ t y}^{-1}$) is almost twice as high as the riverine input ($25 * 10^6 \text{ t y}^{-1}$). However, this estimate was made for the open shelf. In the sheltered estuaries of Ob and Yenisei, we expect lower rates of coastal erosion because erosional energy by waves is minor and thus the coastline is more stable. Furthermore, there is a different type of permafrost along the Kara

Sea coast (International Permafrost Association, Data and Information Working Group, comp. 1998) because no ice complexes are found as described from the Laptev Sea (Schirmer et al., 2002). Such ice complexes commonly contain up to 80% of water which melts during the summer thereby forming unstable sediment cliffs susceptible to coastal erosion. Missing ice complexes in association with a low relief (Gordeev et al., 1996; Milliman and Syvitzky, 1992) suggest that significant coastal erosion is unlikely in the sheltered Ob and Yenisei estuaries.

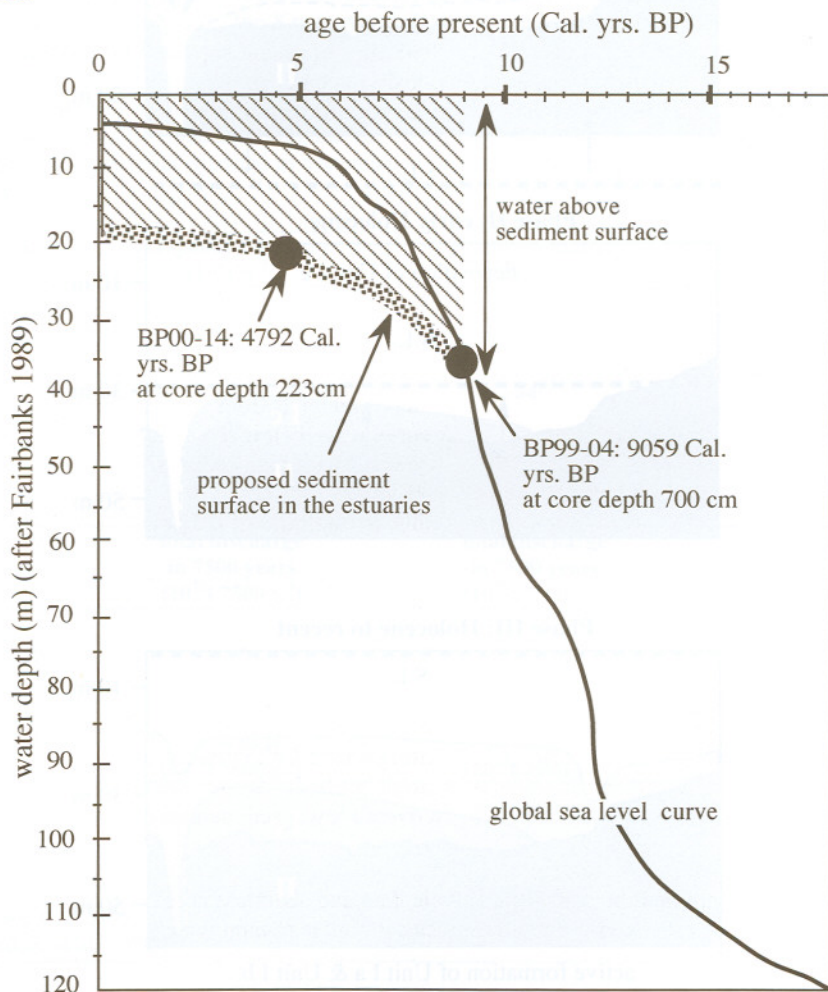


Fig. 14: Eustatic sea-level trend for the last 15000 years (after Barbados sea-level curve by Fairbanks 1989) and reconstructed sediment surface in the Yenisei Estuary after chronological data from cores BP99-04 and BP00-14 (Fig. 9). Note that channel erosion was before and onset of sedimentation after 10 Cal. kyrs. BP. During the Holocene transgression sea-level rise exceeded sediment accumulation in the area of the cores.

If coastal erosion is not important, one simple way of testing our budget is to compare the total net sediment masses estimated from this study with the modern average discharge of suspended and dissolved matter (Gordeev et al., 1996; Telang et al., 1991) extrapolated back over the last 7500 years (Table 2), the time period during which we believe the establishment of the modern marginal filter system has occurred. In order to be closer to Holocene conditions not affected by anthropogenic change, we include data from before A.D. 1950 (Table 2; Telang et al., 1991; Holmes et al., in press) for the Yenisei River. This takes into account dam building (e.g., the Krasnoyarsk Dam) during the last 50 years in the catchment area of the Yenisei Estuary.

Table 2. I: Recent sediment discharge for the Ob and Yenisei rivers. II: Discharge amount of suspended and dissolved matter during the last 7500 years quantified by linear extrapolation of I. III: Total amount of material expected as accumulated sediments present in the marginal filter according to Lisitzin (1995).

I.	suspended matter (10^6 t y^{-1})	dissolved matter (10^6 t y^{-1})	
Ob	16.5 ⁽²⁾ 13.4 ⁽¹⁾		
	15.5	34⁽¹⁾	
Yenisei	5.9 ⁽²⁾ 14.4 ⁽¹⁾		
	14.4	43.2⁽¹⁾	
II.	total discharge in 7500 years ($10^{10} \text{ t 7500 y}^{-1}$)	total discharge in 7500 years ($10^{10} \text{ t 7500 y}^{-1}$)	
Ob	11.6	25.5	
Yenisei	10.8	32.4	
III.	90 % of II ($10^{10} \text{ t 7500 y}^{-1}$)	30 % of II ($10^{10} \text{ t 7500 y}^{-1}$)	
Ob	11.0	7.7	18.7
Yenisei	10.3	9.7	20.0

(1) Telang et al. (1991)
(2) Gordeev et al. (1996)

The extrapolation suggests that the Ob River released $11.6 * 10^{10} \text{ t}$ of suspended matter and $25.5 * 10^{10} \text{ t}$ of dissolved matter during the last 7500 years (Table 2). The Yenisei River discharged $10.8 * 10^{10} \text{ t}$ of suspended matter and $32.4 * 10^{10} \text{ t}$ of dissolved matter (Table 2). According to Lisitzin (1995), 90% of the total suspended matter and 30% of the dissolved matter precipitate and accumulate in the marginal filter at the river-sea interface. If true, this would result in a total sediment accumulation of $18.7 * 10^{10} \text{ t}$ for the Ob River and $20 * 10^{10} \text{ t}$

for the Yenisei River (Table 2). These numbers are significantly higher than the Holocene sediment masses estimated from mapping of Unit I sediment thickness in the Ob and Yenisei estuaries which results in $14.3 * 10^{10}$ t (about 75% of the modern-based calculated value), and $9.2 * 10^{10}$ t (about 50% of the modern-based calculated value), respectively (Table 1). It may suggest that the study of Lisitzin (1995) describing the marginal filter as efficient sediment trap for fluvial-derived material underestimates sediment bypass and/or export into the Kara Sea. The discrepancy between our and Lisitzin's approximation is highly relevant for both assessment of material exported from the Ob and Yenisei catchments into the Kara Sea and the sediment budget of the entire Arctic Ocean. Thus, the possible reasons, which can account for the discrepancy, need to be discussed in further detail.

One reason may be that the ELAC system used for our quantification does not penetrate Unit I down to the top of Unit II in all locations thereby underestimating Unit I thickness and mass. This is not very likely because the strong reflector marking the top of Unit II is visible in most profiles (Figs. 4 and 5). Moreover, comparison along lines, where both CHIRP and ELAC data were recorded during the expedition BP01, demonstrate that both systems revealed the same thickness for Unit I (Stein and Stepanets, 2001; Fig. 2).

Another reason may be that the extrapolation of recent run-off data as summarised in Table 2 may not be correct and/or not valid for the last 7500 years because climate change could have caused variation in run-off during the Holocene (Stein et al., this volume). Here it is interesting to note that our assessment of sediment accumulation for Subunit Ia for the last 5000 years matches almost exactly recent sedimentation rates in the marginal filter using Cs 137 records (Stepanets et al., 1999). Combining the average porosity (66%) with the mean Subunit Ia sedimentation rate (0.2 cm y^{-1}) and the average sediment surface porosity (74%) with near-surface sedimentation rates of 0.3 cm y^{-1} (Stepanets et al., 1999), respectively, results very similar in mass accumulation rates (MAR) of $0.21 \text{ g cm}^{-2} \text{ kyrs}^{-1}$ in surface sediments and $0.2 \text{ g cm}^{-2} \text{ kyrs}^{-1}$ in the entire Subunit Ia.

Thus, the most reasonable explanation for this discrepancy is that our study does not quantify early Holocene accumulation correctly until ca. 5 to 6 Cal. kyrs. BP, the time when sea level reached the present level. The southward migrating position of the marginal filter during the transgression is difficult to compile from the data available. Possibly, there are additional depositional centers further north, which are outside the area of data acquisition and thus not yet mapped (Stein et al., this volume). The character of a deepening upward sedimentary sequence in the estuaries in association with acoustic pattern indicative for currents in the early Holocene (Figs. 2, 5 and 6) suggest that current-induced bypassing of sediments onto the open Kara Shelf has decreased during the Holocene. In turn, this implies higher sediment export out of the area mapped in this study before 5 Cal. kyrs. BP. This export must have been significant because Subunit Ic sediments, interpreted as fluvial deposits possibly older than 8 Cal. kyrs. BP, are included in the budget based on mapping. Therefore, our approach using the total thickness of Unit I sediments should overestimate the actual budget for the last 7500 years thereby increasing the discrepancy between the different ways of quantification.

Although early Holocene bypass probably accounts for most of the budget discrepancy discussed above, sediment export out of the estuaries may also play some role today and during the last 5000 years. Is there evidence for sediment erosion and lateral transport?

Ice gouges visible in the acoustic images are evidence for grounded ice floes (Fig. 2) which can disperse sediment at the bottom (Barnes and Lien, 1987; Reimnitz et al., 1972;

1978) when drifting sea ice ridges plough through the sediment. Ice thickness can reach up to 20 m in pressure ridges (Løset et al., 1999; Barnes and Lien, 1987). However, at least for the area of Ob and Yenisei estuaries sediments appear mostly undisturbed in acoustic images and ice gouges only occur locally (Fig. 2). Therefore, ice gouging is expected to play only a minor role in the sediment budget of the Ob and Yenisei marginal filter systems.

Sediment bypass may be enhanced by bottom currents which can be provoked by tidal activity, changes in the river discharge (especially at the spring discharge peak), and brine formation by freezing of seawater (Reimnitz et al., 1993; Dethleff, 1994; Løset et al., 1999; Barnes and Lien, 1987; Lisitzin, 1995; Pfirman et al., 1995; Are, 1996). Evidence from this and other studies suggest that, at least for the Yenisei Estuary, considerable bypass has to be considered for the present situation of the marginal filter. Material export along certain pathways out of the Yenisei Estuary is documented by relatively high values of magnetic susceptibility in surface sediments on the open Kara shelf, mainly concentrated in morphological depressions and/or channels (Fig. 13; Stein et al., this volume). This is consistent with the fact that in cores from the area north of the Yenisei marginal filter (BP00-36, BP00-26, and BP00-07) there is still accumulation today, but with smaller rates of 7, 17 and 40 ($\text{g cm}^{-2} \text{ky}^{-1}$), respectively, compared to the early Holocene. Moreover, according to our estimates, there is a smaller Holocene sediment mass in the Yenisei Estuary (Table 1) than in the Ob Estuary although they receive nearly the same influx (Table 2). Thus, accumulation rates, magnetic susceptibility in surface sediments and the sediment budget indicates some unquantified sediment export from the Yenisei Estuary to the shelf probably active during the entire last 5000 years.

Higher export rates of particulate matter out of the Yenisei Estuary could be related to different estuarine morphologies and hydrological regimes. It is interesting to note that inflow of sea water into the Yenisei Estuary is enhanced by its deeper bathymetry compared to that of the Ob. Harms et al. (this volume) describe a strong sea water underflow in the Yenisei as a result of channelled river water inflow into the Kara Sea which is of the same direction as the main summer winds thereby enforcing Ekman transport. Thus, through the Yenisei Estuary surface waters are transported relatively far to the north. In contrast, the mouth of the Ob Estuary is characterised by a tide-wave interference zone with relatively high kinetic energies which may influence sediment transport, mixing, and deposition in relatively unstratified waters (Harms et al., this volume). These different characteristics may result in a larger sediment export to the open shelf out of the Yenisei Estuary as compared to the Ob.

5 Conclusions

The sediments in the Ob and Yenisei estuaries can be divided into two major acoustic and lithological Units (I and II). Unit II forms the pre-Holocene basement with little acoustic penetration. During the last sea-level lowstand, the erosional surface was formed on top of this unit including several incised river channels. The younger Unit I can be divided into three subunits, Ia to Ic. Their formation is related to post glacial sea-level rise after about 12 Cal. kys. BP and the southward migration of the river-sea marginal filters to their recent position in the estuaries between 72° to 73° N. The lowermost subunits Ic and Ib show fluvial to shallow-marine seismic features comparable to typical channel-levee-complexes representing a fine-grained meandering river depositional environment overlain by a transgressive system tract and finally high stand system tract after about 5 Cal. kys. BP. The entire sediment fill of

the present estuaries reflects a deepening-upward sediment growth structure suggesting that sea-level rise exceeded sediment accumulation although migration of the marginal filter during the Holocene shifted depositional centers south.

The present estuaries of the Ob and Yenisei rivers are the major Holocene sediment sinks of terrigenous material supplied by rivers. An estimated total of 14.3×10^{10} t and 9.2×10^{10} t of dry sediment have accumulated during the Holocene, which is about 75% and 50% of the material expected from extrapolation of modern run-off data, respectively. Sediment deposition in early Holocene times outside the recent position of the marginal filter is proposed to be the reason for the differences in the sediment budgets. A progressive southward migration of the position of the marginal filter in response to the elevating sea level is favoured to account for the "missing" material. This would mean that a significant amount of material was deposited on the present shelf and not in the position of the recent marginal filter. Extensive sediment reworking is not observed but significant sediment bypass through the marginal filter system cannot be excluded. Further studies are necessary to improve the temporal and spatial resolution of Holocene sediments for a better assessment of the early Holocene budget particularly in the central and northern areas of the Kara Sea.

The existence of filled paleoriver channels suggests a pre-Holocene history of the southern Kara Sea shelf similar to that in the Laptev Sea (Kleiber and Niessen 1999). These channels must have been eroded during the sea-level lowstand and were filled with sediments during the Holocene transgression. River erosion of the exposed shelf of the southern Kara Sea during implies continuous river transport across the shelf and absence of an ice sheet in the area of channel erosion.

Acknowledgements

Many thanks to J. Matthiessen and V. Rachold for their helpful comments. A special thanks to Frank Schoster and Mathias Kraus for many fruitful discussions. This study has been performed within the German-Russian research project "Siberian River Run-Off (SIRRO)", Financial support by the German Ministry of Education, science, Research and Technology (BMBF) (grant no. 03G0547A) and the Russian Foundation of Basic research is gratefully acknowledged. We are also grateful to the crew of RV "Akademik Boris Petrov" for their support. Review comments of L. Polyak and R. Endler were highly appreciated and improved an earlier version of the paper considerably.

References

- Aagaard, K., Carmack, E.C., 1989. The role of sea ice and other fresh water in the Arctic circulation. *J. Geophys. Res.* 94, C10, 14485-14498.
- Allen, J.R.L., 1965. A review of the origin and characteristics of recent alluvial sediments. *Sedimentology* 5, 89-191.
- AMAP, 1998. AMAP assessment report: Arctic pollution issues. Arctic Monitoring and Assessment Programme (AMAP), Oslo, Norway, 859 pp.
- Are, F. E., 1996. Dynamics of the littoral zone of Arctic Seas (State of the art and goals). *Polarforschung* 64 (3) 123-131.

- Bally, A.W., 1987. Atlas of Seismic Stratigraphy. AAPG Studies in Geology, 27 (Vol.1). The American Association of Petroleum Geologists, Tulsa 125pp.
- Bauch, H.A., Kassens, H., Naidina, O.D., Kunz-Pirrung, M., Thiede, J., 2000. Composition and Flux of Holocene Sediments on the Eastern Laptev Sea Shelf, Arctic Siberia. *Quat. Res.* 55 (3) 344-351.
- Bauch, H. A., Mueller-Lupp, T., Taldenkova, E., Spielhagen, R. F., Kassens, H., Grootes, P.M., Thiede, J., Heinemeier, J., Petryashov, V.V., 2001. Chronology of the Holocene transgression at the North Siberian margin. *Glo. Plan. Change* 31, 125-139.
- Barnes, P.W., Lien, R., 1987. Icebergs rework sediments on Antarctic shelf. *Antarctic Journal of the United States* 22 (5) Review, 130-131.
- Blanchet, D., Bhat, S.U., Wilkman, G., 1995. Ice conditions in the Ob Bay in western Siberia. International Symposium on Ice, 14th, Potsdam, NY, July 27-31, 1998. Proceedings. Ice in surface waters. Vol.1. Edited by H.T. Shen: Rotterdam, A.A. Balkema, 1998, 259-267.
- Bown, T.M., Kraus, M.J., 1987. Integration of channel and floodplain sites, I. Development of sequences and lateral relations of alluvial paleosols. *J. Sed. Petrol.* 57, 587-601.
- Brierley, G.J., Ferguson, R.J., Woolfe, K.J., 1997. What is a fluvial levee? *Sed. Geol.* 114, 1-9.
- Damuth, J.E., 1975. Echo character of the western equatorial Atlantic floor and its relationship to the dispersal and distribution of terrigenous sediments. *Mar. Geol.* 18, 17-45.
- Damuth, J.E., 1978. Echo character of the Norwegian-Greenland Sea: relationship to Quaternary sedimentation. *Mar. Geol.* 28, 1-36.
- Dearing, J., 1994. Environmental magnetic susceptibility - using the Bartington MS2 system. Chi Publishing, Kenilworth, UK
- Dethleff, D., 1994. Dynamics of the Laptev Sea flaw lead. *Berichte zur Polarforschung - Rep. Pol. Res.* 144, 49-54.
- Dyer, K.R., 1986. Coastal and estuarine sediment dynamics. Wiley and Sons, New York, 342pp.
- Fader, G.B.J., 1997. The Effects of shallow Gas on Seismic Reflection Profiles. In Davies, T. A. et al. (Eds.) *Glaciated continental margins: an atlas of acoustic images*. London: Chapman and Hall, 315pp.
- Fairbanks, R. G., 1989. A 17,000-year glacio-eustatic sea-level record: influence of glacial melting rates on the Younger Dryas event and deep ocean circulation. *Nature* 342, 637-642.
- Galloway, W.E., Hobday, D.K., 1996. Terrigenous clastic depositional systems. Springer 489pp.
- Gordeev, V.V., Martin, J.M., Sidorov, I.S., Sidorova, M.V., 1996. Reassessment of the Eurasian river input of water, sediment, major elements, and nutrients to the Arctic Ocean. *Am. J. Sci.* 296 (6) 664-691.
- Grebmeier, J.M., 1995. Biological processes on Arctic continental shelves, Ice-ocean-biotic interactions, in Smith, W.O., Grebmeier, J.M., (Eds.) *Arctic oceanography: Marginal ices zones and continental shelves: Coastal and Estuarine studies* 49, 231-261.
- Hamilton, E.L., 1972. Compressional-wave attenuation in marine sediments. *Geophysics* 37, 620-646.
- Holmes, R. M., McClelland, J. W., Peterson, B. J., Shiklomanov, A. I., Zhulidov, A.V., Gordeev, V.V., Bobrovitskaya, N., 2002. A circumpolar perspective on fluvial sediment flux to the Arctic Ocean. *Global Biogeochemical Cycles*, in press.

- International Permafrost Association, Data and Information Working Group, comp. 1998. Circumpolar Active-Layer Permafrost System (CAPS), version 1.0. Boulder, CO: National Snow and Ice Data Center/World Data Center for Glaciology. CD ROM.
- Kleiber, H.-P., Niessen, F., 2000. Variations of continental discharge pattern in space and time: Implications from the Laptev Sea continental margin, Arctic Siberia: *Int. J. E.Sci.* 89, 605-616.
- Lisitzin, A. P., 1995. The marginal filter of the ocean. *Oceanology* 34 (5) 671-682.
- Løset, S., Shkhinek, K., Gudmestad, O.T., Strass, P., Michalenko, T., Frederking, R., Kärnä, T., 1999. Comparison of the physical environment of some Arctic seas. *Cold Reg. Sci. Tech.* 29 (3) 201-214.
- Macdonald, R.W., Solomon, S.M., Cranston, R.E., Welch, H.E., Yunker, M.B., Gobeil, C., 1998. A sediment and organic carbon budget for the Canadian Beaufort Shelf. *Mar. Geol.* 144, 255-273.
- Matthiessen, J., Stepanets, O. V., 1999. The expedition to the Kara Sea in summer 1997: Summary of the shipboard scientific results. The Kara Sea Expedition of RV "Akademik Boris Petrov" 1997: First results of a joint Russian-German pilot study. *Rep. Pol. Res.* 300, 5-16.
- Miall, A.D., 1996. The geology of fluvial deposits. Springer, 582pp.
- Milliman, J.D., Syvitsky, P.M., 1992. Geomorphic/Tectonic Control of Sediment discharge to the Ocean: The importance of Small Mountainous Rivers. *Geology* 100 (5) 525-544.
- Mitchum, R.M.Jr., Vail, P.R., Thompson, S., 1977. In *Seismic stratigraphy and global changes of sea level; Part 2, The depositional sequence as a basic unit for stratigraphic analysis: Seismic stratigraphy; applications to hydrocarbon exploration.* Am. Assoc. Petr. Geol. 26, 53-62.
- Niessen, F., Weiel, D., 1996. Distribution of magnetic susceptibility on the Eurasian shelf and continental slope - implications for source areas of magnetic minerals. In: Stein, R., Ivanov, G.I., Levitan, M.A., Fahl, K. (eds) *Surface-sediment composition and sedimentary processes in the central Arctic Ocean and along the Eurasian Continental Margin.* *Rep. Pol. Res.* 149, 81-88.
- Pavlov, V.K., Pfirman, S.L., 1995. Hydrographic structure and variability of the Kara Sea: Implications for pollutant distribution. *Deep-Sea Res. II* 42, 1369-1390.
- Pfirman, S. L., Kögeler, J., Anselme, B., 1995. Coastal environments of the western Kara and eastern Barents Seas. *Deep-Sea Res. II* 42, 391-1412.
- Polyak, L., Levitan, M., Gataullin, V., Khusid, T., Mikhailov, V., Mukhina, V., 2000. The impact of glaciation, river-discharge and sea-level change on Late Quaternary environments in the south-western Kara Sea. *Int. J. Earth Sci.* 89, 550-562.
- Rachold, V., Grigoriev, M.N., Bauch, H.A., 2000. Coastal erosion vs. riverine sediment discharge in the Arctic Shelf seas. *Int. J. Earth Sci.* 89, 450-460.
- Rachold, V., Eicken, H., Gordeev, V.V., Grigoriev, M.N., Hubberten, H.-W., Lisitzin, A.P., Shevchenko, V.P., Schirrmeister, L., 2003. Modern terrigenous organic carbon input into the Arctic Ocean. In: R. Stein and R.W. Macdonald (Eds.). *The Arctic Ocean Organic Carbon Cycles: Present and Past.* Springer Verlag Berlin, in press.
- Reimnitz, E., McCormick, M., McDougall, K., Brouwers, E.M., 1993. Sediment export by ice rafting from a coastal polynia, Arctic Alaska, U.S.A. *Arc. Alp. Res.* 25, 83-98.
- Reimnitz, E., Toimil, L., Barnes, P., 1978. Arctic continental shelf Morphology related to sea ice-zonation, Beaufort Sea, Alaska. *Mar. Geol.* 28, 179-210.

- Reimnitz, E., Barnes, P., Forgatsch, T., Rodeick, C., 1972. Influence of grounding ice on the Arctic Shelf of Alaska. *Mar. Geol.* 13, 323-334.
- Schirmermeister, L., Siegert, Ch., Kunitzky, V.V., Grootes, P.M., Erlenkeuser, H., 2002. Late Quaternary ice-rich permafrost sequences as a paleoenvironmental archive for the Laptev Sea Region in northern Siberia. *Int. J. Earth Sci.* 91, 154-168.
- Schultheiss, P.J., Mienert, J., 1987. Whole-core p-wave velocity and gamma-ray attenuation logs from Leg 108 (sites 657 through 668). In: Ruddiman, M. Sarntheim et al. (Eds.), *Proc. ODP Init. Rep.*, 108, 1015-1017.
- Schultheiss, P.J., McPhail, S.D., 1989. An automated p-wave logger for recording fine scale compressional wave velocity in sediments. In: W. Ruddiman, M. Sarntheim et al. (Eds.), *Proc. ODP Init. Rep.* 108, 407-413.
- Shiklomanov, I. A., Skakalsky, B. G., 1994. Studying water, sediment and contaminant runoff of Siberian Rivers. *Modern Status and prospects. Arc. Res. U.S.* 8, 295-306.
- Stein, R., 1991. Accumulation of Organic Carbon in marine sediments. *Lecture Notes in Earth Sciences.* 34, 217pp.
- Stein, R., Fahl, K., 2000. Holocene Accumulation of Organic Carbon at the Laptev Continental Margin (Arctic Ocean): Sources, pathways, and sinks. *Geo-Mar. Lett.*, 20, 27-36.
- Stein, R., Stepanets, O., 2000. Scientific Cruise Report of the Joint Russian-German Kara Sea Expedition of RV "Akademik Boris Petrov" in 1999. *Rep. Pol. Res.* 360, 142pp.
- Stein, R., Stepanets, O., 2001. Scientific Cruise Report of the Joint Russian-German Kara Sea Expedition of RV "Akademik Boris Petrov" in 2000. *Rep. Pol. Mar. Res.* 393, 287pp.
- Stein, R., Stepanets, O., 2002. Scientific Cruise Report of the Joint Russian-German Kara Sea Expedition of RV "Akademik Boris Petrov" in 2001. *Rep. Pol. Mar. Res.* 419, 278pp.
- Stein, R. Macdonald, R.W., 2003. *The Arctic Ocean Organic Carbon Cycles: Present and Past.* Springer Verlag Berlin, in press.
- Stepanets, O.V., Borisov, A.P., Soloveva, G.Y., 1999. Distribution of anthropogenic radionuclides in the estuaries of Ob and Yenisei rivers and adjacent Kara Sea. *Rep. Pol. Mar. Res.* 300, 132-141.
- Telang, S. A., Pocklington, R., Naidu, A.S., Romankevich, A.E., Gitelson, I.I., Gladdyshv, M.I., 1991. Carbon and mineral transport in major North American, Russian Arctic, and Siberian rivers: The St. Lawrence, the Mackenzie, the Yukon, the Arctic Alaskan rivers, the Arctic Basin rivers in the Soviet Union, and the Yenisei. *Biogeochemistry of major World Rivers.* In: Degens, E. T., Kempe, S, Richey, J.E. Chichester, New York, Brisbane, Toronto, Singapore, Wiley and Sons. Scope 42, 75-104.
- Thompson, R., Oldfield, F., 1986. *Environmental Magnetism.* Allen and Unwin, London, 205pp.
- Thorne, J.A., Swift, D.J.P., 1991. Sedimentation on continental margins, VI: a regime model for depositional sequences, their component system tracts, and bounding surfaces. In: Swift, D.J.P. Oertel, G.F., Tillman, R.W. Thorne, J.A. (Eds.). *Shelf Sand and Sandstone Bodies. Geometry Facies and Sequence Stratigraphy: Spec. Publ. Int. Assoc. Sedimentl.* 14, 189-255.
- Vail, P.R., Mitchum, R.M., Todd, R.G., Widmier, J.M., Thompson, S., Sangree, J.B., Bubb, J.N., Hatelid, W.G., 1977. Seismic stratigraphy and global changes of sea-level. *Am. Assoc. Petr. Geol.* 26, 49-212.

- Weaver, P.P.E., Schultheiss, P.J., 1990. Current methods for obtaining, logging and splitting marine sediment cores. *Mar. Geophys. Res.* 12, 85-100.
- Weber, M. E., Niessen, F., Kuhn, G., Wiedicke, M., 1997. Calibration and application of marine sedimentary physical properties using a multi-sensor core logger. *Mar. Geol.* 136, 151-172.